Demonstration of Impedance Matching Using a mu-Negative (MNG) Metamaterial

R. B. Greegor,　C. G. Parazzoli,　J. A. Nielsen,　M. H. Tanielian,　D. C. Vier,　S. Schultz,
Christopher L. Holloway, *Senior Member, IEEE*, and Richard W. Ziolkowski, *Fellow, IEEE*

Abstract—A mu-negative (MNG) metamaterial hemisphere was used to demonstrate impedance matching for a magnetic loop. The metamaterial was comprised of copper spirals deposited on an alumina substrate. The spirals, hemisphere, and magnetic loop were designed to operate at ∼450 MHz. The effect of the metamaterial hemisphere was to improve the match of the electrically small loop antenna to the power source impedance increasing the overall radiated power. Results show a 17-dB increase in total radiated power relative to the bare loop. This was lower than anticipated due to losses in the MNG hemisphere.

Index Terms—Antenna, electrically small, magnetic loop, metamaterial.

I. INTRODUCTION

IN 1968, Veselago [1] discussed the possibility of a negative index of refraction material having both an effective negative permittivity ε_{eff} and permeability μ_{eff} (i.e., a double negative (DNG) metamaterial). More recently, this material was realized by appropriately depositing split rings and wires on a dielectric substrate [2], [3]. The ring and wire DNG metamaterial was used to construct a Snell's Law wedge that verified the existence of the negative index, n [3], [4]. Since then, we have fabricated DNG split ring and wire structures operating in the super high frequency (SHF) RF region for a cylindrical lens [5], a one-dimensional (1D) graded index lens [6], a lens with spherical curvature, and a two-dimensional (2D) graded index lens [7]. These lenses have the advantage of being lighter and having lower aberrations than RF lenses constructed of conventional materials such as Rexolite [8]. In addition to the SHF unit cells for the lens applications mentioned above, we have developed highly subwavelength, low loss lumped-element based unit cells to realize a DNG medium in the UHF regime [9], [10].

R. B. Greegor, C. G. Parazzoli, J. A. Nielsen, and M. H. Tanielian are with Boeing Phantom Works, Seattle, WA 98124 USA (e-mail: robert.b.greegor@boeing.com; claudio.g.parazzoli@boeing.com; jean.a.nielsen@boeing.com; minas.h.tanielian@boeing).

D. C. Vier and S. Schultz are with the Department of Physics, University of California, San Diego, La Jolla, CA 92093 USA (e-mail: dvier@ucsd.edu; sschultz@ucsd.edu).

C. L. Holloway is with the National Institute of Standards and Technology, U.S. Department of Commerce, Boulder, CO 80305 USA (e-mail: holloway@boulder.nist.gov).

R. W. Ziolkowski is with the Department of Electrical and Computer Engineering, University of Arizona, Tucson, AZ 85721 USA (e-mail: ziolkowski@ece.arizona.edu).

Besides DNG mediums, there are also single negative (SNG) metamaterials, where either the real part of the permittivity or permeability is negative. In particular, DNG or SNG metamaterials have been used to achieve efficient electrically small antennas (ESAs) [11]–[14]. The predictions [11]–[13] have been based on a metamaterial shell surrounding an electric dipole with a shell radius r on the order of 2.0 cm for operation at 300 MHz, so that $r \sim \lambda/50$. Nearly complete matching was achieved with the metamaterial shell alone, without the presence of an external matching circuit. The metamaterial required for several of the reported cases is either a DNG with the real part of the index of refraction $n' = -3.0$ or an SNG with the real part of the permittivity $\varepsilon' = -3.0$.

The desire for ESAs has obvious applications, including mobile communications, RF-tagging, and wireless networking. From a fundamental standpoint it is well understood that as the antenna becomes electrically small (i.e., $ka < 0.5$ where k is the free space wave number and a is the radius of the smallest sphere enclosing the antenna), its impedance is poorly matched to the source and the bandwidth is substantially reduced. This bandwidth performance limitation is related to the Chu limit for the quality factor. In particular, the lower bound on the quality factor is given by [15], [16]

$$Q_{lb} \geq \eta \left[\frac{1}{(ka)^3} + \frac{1}{ka} \right]$$

where η is the frequency dependent radiation efficiency of the antenna. In the absence of losses, the quality factor Q is proportional to the ratio of ω times the stored energy to the power radiated by the antenna. It is desirable to have Q as low as possible in order to have as high as possible fractional bandwidth, which is given by $FBW \sim 2/Q$. However, the Chu limit shows that as ka becomes small, the Q increases. Hence, achieving a wide bandwidth for an ESA has proven to be challenging.

In this letter, we report a proof-of-principle for an impedance-matching electrically small MNG ($\mu' < 0$) metamaterial hemisphere around an even smaller magnetic loop antenna operating at 430 MHz. We describe the design of the metamaterial hemisphere, the spiral unit cell introduced to construct it, and the resulting performance characteristics of the overall antenna system. We compare these results to those of the bare magnetic loop to demonstrate the ability of the metamaterial hemisphere to act as a matching element. We also compare the bandwidth results to the Chu limit. Our efforts to minimize the losses of this ESA system will also be described as well as the impact of the fabrication and measurement errors on them.
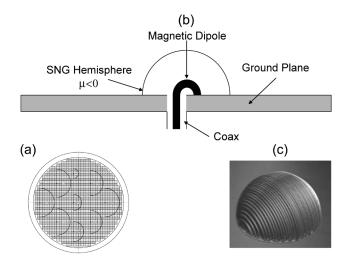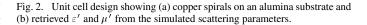
Fig. 1. Components of the hemispherical ESA: (a) unit cell position on the alumina wafer showing the laser cutting contours, (b) cross-section showing the coaxial feed, ground plane, magnetic loop, and MNG hemisphere, and (c) final assembly of stacked slices forming a hemisphere around the magnetic loop.

II. HEMISPHERICAL ANTENNA DESIGN

The configuration of the hemispherical ESA is shown in Fig. 1. A 0.9-cm radius magnetic loop is fed through a ground plane by the center conductor of a SMA connector. The MNG copper spirals were deposited on an alumina wafer in a square periodic array pattern. As illustrated in Fig. 1(a), the wafer was laser cut into semicircles of different radii. The semicircles were stacked to form a hemisphere that was placed over the magnetic loop, but which was also easily removed to facilitate measurements in its absence. The nominal radius of the hemisphere design was 1.8 cm. However, the wafer thickness was slightly larger than the desired value of 0.1 cm, and the wafer radii were larger due to the laser cutting step in the fabrication process. Consequently, the actual radius perpendicular to the stacking plane was closer to 2.0 cm, and the radius in the stacking planes was closer to 1.9 cm.

The unit cell design given in Fig. 2(a) was simulated using Microwave Studio [17] and HFSS [18]. It is comprised of a 7-turn spiral copper conductor whose cross-section is $40~\mu\text{m} \times 40~\mu\text{m}$ with a 50-μm gap between its turns. The copper spiral is on a 1.0-mm thick alumina substrate having $\varepsilon' = 9.9$ and a loss tangent $\delta \sim 10^{-4}$. The nominal overall unit cell size is $3~\text{mm} \times 3~\text{mm} \times 1~\text{mm}$. In the simulations we made the spirals symmetric with respect to the direction of propagation (H is perpendicular to the plane containing the spirals; E lies in the plane of the spirals). This choice made the retrieval of the unit cell parameters from the simulated scattering parameters more accurate than when the spirals were highly asymmetric with respect to the propagation direction. The parameters of the spirals (number of turns, thickness, and spacing), as well as the substrate material, were varied to minimize the loss of the unit cell, while achieving the real part of the permeability $\mu' = -3.0$ at ~450 MHz. Reduction of the unit cell loss is important in order to maximize the total efficiency of the ESA. Finally, we note that this unit cell is only 1D in the sense that it has $\mu' < 0$ only along the axis perpendicular to the

Fig. 2. Unit cell design showing (a) copper spirals on an alumina substrate and (b) retrieved ε' and μ' from the simulated scattering parameters.

spiral plane. We refer to this structure as 1H, as opposed to 3H for which three orthogonal spiral planes would be present.

The values of ε' and μ' retrieved from the simulated scattering parameters are shown in Fig. 2(b). The procedure [19] for extracting these values has been discussed in detail elsewhere. Note that the design also produces $\varepsilon' \sim 40$ in the frequency range of interest and that the value $\mu' = -3$ at ~450 MHz arises from the strong resonance of the copper spirals at ~425 MHz. For the fabricated unit cells, the actual average height of the copper conductors was $\sim 35~\mu$m instead of the design value of $40~\mu$m. This has the effect of reducing the capacitance of the spirals, causing them to resonate at a slightly higher frequency. Our simulations have shown that the resulting smaller copper conductor cross-section leads to higher resistance and, hence, greater ohmic losses. Also, the unit cells on the perimeter of the semicircles were truncated in the laser cutting process. This results in fewer spiral turns, which causes a higher resonant frequency for the hemisphere. The alumina substrate thickness was 1.1 mm instead of the design thickness of 1.0 mm. This additionally leads to a reduction in the capacitance with a concurrent increase in the resonant frequency and the overall losses. We cannot accurately model all of the random fabrication effects, but our simulations indicated that the resonant frequency of the composite hemisphere could be shifted upward as much as 100 MHz from its design value by these fabrication anomalies.

The retrieved values of the ε and μ dispersion relations were used in a COMSOL Multiphysics [20] effective medium simulation of the hemispherical ESA. In the effective medium simulation, the hemisphere was modeled as having uniform properties, i.e., the individual spiral unit cells were not modeled.

This approach was elected because of the prohibitive meshing requirements associated with accurately discretizing hundreds of spirals having micron dimensions in an approximate 12-cm^3 volume. Such an effective medium simulation is useful as an indicator of how the ESA will perform. Our first series of simulations modeled a 3H hemisphere composed of an isotropic effective medium which had the same $\mu' < 0$ along all 3 coordinate axes and a smooth outer surface. These simulations were run to find the optimum radius of the hemisphere to achieve nearly complete matching to a 50-Ω source. However, in reality, the surface of the fabricated metamaterial hemisphere was not smooth, but stair-stepped due to the discrete nature of the square unit cells. Inclusion of this stair-stepping was then taken into account in a simulation series guided by the first idealized set. These results are shown in Fig. 3(a). An improvement of 30 dB at ~450 MHz in the total power radiated by the hemisphere-covered 0.9-cm radius magnetic loop was achieved relative to the same bare magnetic loop without an external matching circuit. The degree of improvement was found to level off for a hemisphere radius of ~1.8 cm. Consequently, this radial value was selected for the design of the fabricated MNG hemispherical ESA. It was found that smaller radial values led to an increased fraction of truncated unit cells on the surface, while larger radial values did not significantly improve the ESA performance. Further simulations included the anisotropic nature of the actual unit cell (i.e., 1H instead of 3H), but they did not show any degradation in the antenna performance. This 1H versus 3H effect was observed before in our previous RF lens designs [6]. It is related to the indefinite nature [21] of the anisotropic 1D or 2D unit cells. Since lower dimensional cells are much simpler to fabricate and exhibit less loss, the 1D cells were preferred over the full 3D ones, especially since they did not significantly alter the ESA performance.

III. MEASUREMENTS RESULTS AND DISCUSSION

On the basis of the simulations, an ESA was fabricated using the spiral unit cell, magnetic loop, and MNG metamaterial hemisphere described above. After fabrication, the antenna performance was measured at NIST-Boulder using a reverberation chamber [22]–[24]. Placing the ESA on a 45.7 cm × 45.7 cm ground plane at the center of the chamber or attaching it to the wall gave essentially the same result. A reverberation chamber is basically an electromagnetically shielded room having an arbitrarily shaped, asymmetric metallic rotating paddle which creates a continuously changing boundary condition in order to generate a statistical electromagnetic (EM) field test environment within the chamber. It provides an ideal environment for measuring the total radiated power of an antenna [22], [25] relative to a reference source and has measurement uncertainties below 1 dB [24].

The hemispherical ESA measurements were compared to the total radiated power of a standard rectangular dual-ridged horn. The same measurements for the bare magnetic loop were made. No external matching circuit was included in either case. This allowed a direct observation of the ability of the MNG hemisphere to act as the matching element. Fig. 3(b) shows the result of combining these two measurements to obtain the total radiated power of the hemispherical ESA compared to the bare mag-
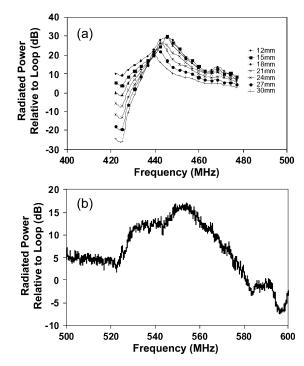

Fig. 3. (a) Simulated total radiated power of a hemispherical ESA with respect to the bare magnetic loop ($r = 0.9$ cm) used to drive the antenna. (b) Measured total radiated power relative to the bare loop.

netic loop used to drive it. Note that the resonance frequency of the measured data was shifted higher by ~100 MHz compared to the simulation values. As argued above, this shift is due to the differences in the ideal simulation geometry versus the actual fabrication tolerances. The measurement shows a resonant improvement of ~17 dB in the total radiated power of the hemispherical ESA as compared to the bare 0.9-cm loop. The measured reflection scattering parameter, S_{11}, was -13.5 dB so that ~96% of the power was accepted by the ESA. In contrast to the expected ~30-dB improvement for the ideal hemispherical ESA, the lower observed value is due to internal, mainly ohmic losses of the MNG metamaterial. In this regard, the resulting ESA was not as efficient a radiator as predicted (our measurements indicate a ~5% radiation efficiency) even though it does provide a good resonant match to the power supply.

For our hemispherical ESA, $ka = 0.23$ at the operating frequency of 550 MHz so that the Chu limit is $Q_{\mathrm{Chu}} = 0.05[1/(0.23)^3 + 1/(0.23)] = 4.33$. Hence, the Chu fractional bandwidth is $FBW_{\mathrm{Chu}} = 2/Q_{\mathrm{Chu}} = 0.462$. From Fig. 3(b) the measured fractional bandwidth (using the -3 dB points) is $FBW_{\mathrm{Meas}} \sim 14/550 = 2.55 \times 10^{-2}$. The corresponding quality factor is $Q_{\mathrm{Meas}} = 78.4$, about 18.1 times the Chu limit. Obviously the bandwidth is larger when losses are present, but by including the radiation efficiency this advantage is eliminated. The low radiation efficiency is due to the large unit cell losses which concurrently broaden the ESA bandwidth.

IV. CONCLUSION

In conclusion, we have shown that the placement of a hemispherical MNG, $\mu' < 0$, metamaterial around a bare magnetic loop significantly improves its match to the source and, hence,

its total radiated power. The ESA was measured to have a resonant total radiated power enhancement of ∼17 dB above the bare magnetic loop. The MNG hemisphere acted as a matching element so that ∼96% of the source power was accepted by the antenna. Unfortunately, the unit cell losses prevented achieving the numerically predicted improvement of ∼30 dB. On the other hand, they significantly broadened the bandwidth of the hemispherical ESA response. While the principle of radiative enhancement using MNG metamaterials has been demonstrated, the practical realization of this concept awaits further improvements in low loss unit cell designs, at least for the geometries considered here.

ACKNOWLEDGMENT

REFERENCES

[1] V. G. Veselago, "The electrodynamics of substances with simultaneously negative values of ε and μ," *Sov. Phys. Usp.*, vol. 10, pp. 509–514, 1968.

[2] D. R. Smith, W. J. Padilla, D. C. Vier, S. C. Nemat-Nasser, and S. Schultz, "Composite medium with simultaneously negative permeability and permittivity," *Phys. Rev. Lett.*, vol. 84, no. 18, pp. 4184–4187, May 2000.

[3] R. A. Shelby, D. R. Smith, and S. Schultz, "Experimental verification of negative index of refraction," *Science*, vol. 292, pp. 77–79, Apr. 2001.

[4] C. G. Parazzoli, R. B. Greegor, K. Li, B. E. C. Koltenbah, and M. H. Tanielian, "Experimental verification and simulation of negative index of refraction using Snell's law," *Phys. Rev. Lett.*, vol. 90, no. 10, Mar. 2003, 107401.

[5] C. G. Parazzoli, R. B. Greegor, J. A. Nielsen, M. A. Thompson, K. Li, A. M. Vetter, and M. H. Tanielian, "Performance of a negative index of refraction lens," *Appl. Phys. Lett.*, vol. 84, no. 17, pp. 3232–3234, Apr. 2004.

[6] R. B. Greegor, C. G. Parazzoli, J. A. Nielsen, M. A. Thompson, M. H. Tanielian, and D. R. Smith, "Simulation and testing of a graded negative index of refraction lens," *Appl. Phys. Lett.*, p. 87, Aug. 2005, 091114.

[7] R. B. Greegor, C. G. Parazzoli, J. A. Nielsen, M. A. Thompson, M. H. Tanielian, D. C. Vier, S. Schultz, D. R. Smith, and D. Schurig, "Microwave focusing and beam collimation using negative index of refraction lenses," *IET Proc. Microw., Antennas, Propag.*, vol. 1, pp. 108–115, Feb. 2007.

[8] C. G. Parazzoli, B. E. C. Koltenbah, R. B. Greegor, T. A. Lam, and M. H. Tanielian, "Eikonal equation for a general anisotropic or chiral medium: Application to a negative-graded index-of-refraction lens with an anisotropic material," *J. Opt. Soc. Amer. B*, vol. 23, no. 3, pp. 439–450, Mar. 2006.

[9] A. Erentok, R. W. Ziolkowski, J. A. Nielsen, R. B. Greegor, C. G. Parazzoli, M. H. Tanielian, S. A. Cummer, B. I. Popa, T. Hand, D. C. Vier, and S. Schultz, "Low frequency lumped element-based negative index metamaterial," *Appl. Phys. Lett.*, vol. 91, Nov. 2007, 184104.

[10] A. Erentok, R. W. Ziolkowski, J. A. Nielsen, R. B. Greegor, C. G. Parazzoli, M. H. Tanielian, S. A. Cummer, B. I. Popa, T. Hand, D. C. Vier, and S. Schultz, "Lumped element-based, highly sub-wavelength negative index metamaterials at UHF frequencies," *J. Appl. Phys.*, vol. 104, no. 3, Aug. 2008, 034901.

[11] R. W. Ziolkowski and A. Erentok, "Metamaterial-based efficient electrically small antennas," *IEEE Trans. Antennas Propag.*, vol. 54, no. 7, pp. 2113–2130, Jul. 2006.

[12] R. W. Ziolkowski and A. Erentok, "At and below the Chu limit: Passive and active broad bandwidth metamaterial-based electrically small antennas," *IET Proc. Microw., Antennas Propag.*, vol. 1, pp. 116–128, Feb. 2007.

[13] A. Erentok and R. W. Ziolkowski, "A hybrid optimization method to analyze metamaterial-based electrically small antennas," *IEEE Trans. Antennas Propag.*, vol. 55, no. 3, pp. 731–741, Mar. 2007.

[14] H. R. Stuart and A. Pidwerbetsky, "Electrically small antenna elements using negative permittivity resonators," *IEEE Trans. Antennas Propag.*, vol. 54, no. 6, pp. 1644–1653, Jun. 2006.

[15] J. S. McLean, "A re-examination of the fundamental limits on the radiation Q of electrically small antennas," *IEEE Trans. Antennas Propag.*, vol. 44, pp. 672–676, May 1996.

[16] S. R. Best, "Low Q electrically small linear and elliptical polarized spherical dipole antennas," *IEEE Trans. Antennas Propag.*, vol. 53, pp. 1047–1053, Mar. 2005.

[17] Microwave Studio. Computer Simulation Technology (CST) GmbH, Darmstadt, Germany.

[18] HFSS. Ansoft, Pittsburgh, PA.

[19] D. R. Smith, D. C. Vier, T. Koschny, and C. M. Soukoulis, "Electromagnetic parameter retrieval from inhomogeneous metamaterials," *Phys. Rev.*, vol. E 71, Mar. 2005, 036617.

[20] Multiphysics. Comsol AB, Stockholm, Sweden.

[21] D. R. Smith and D. Schurig, "Electromagnetic wave propagation in media with indefinite permittivity and permeability tensors," *Phy. Rev. Lett.*, vol. 90, no. 7, Feb. 2003, 077405.

[22] P. Wilson, G. Koepke, J. Ladbury, and C. L. Holloway, "Emission and immunity standards: Replacing field-at-a-distance measurements with total-radiated-power measurements," in *Proc. IEEE Int. Symp. Electromagn. Compat.*, Aug. 2001, vol. 2, pp. 964–969.

[23] C. L. Holloway, D. A. Hill, J. M. Ladbury, and G. Koepke, "Requirements for an effective reverberation chamber: Unloaded or loaded," *IEEE Trans. Electromagn. Compat.*, vol. 48, no. 1, pp. 187–194, Feb. 2006.

[24] C. L. Holloway, D. A. Hill, J. M. Ladbury, P. Wilson, G. Koepke, and J. Coder, "On the use of reverberation chambers to simulate a controllable Rician radio environment for the testing of wireless devices," *IEEE Trans. Antennas Propag.*, vol. 54, no. 11, pt. 1, pp. 3167–3177, Nov. 2006.

[25] H. G. Krauthauser, "On the measurement of total radiated power in un-calibrated reverberation chambers," *IEEE Trans. Electromagn. Compat.*, vol. 49, no. 2, pp. 270–279, May 2007.